ENGINEER - Vol. LIX, No. 02, pp. [21- 30], 2026

DOI: https://doi.org/10.4038/engineer.v59i2.7746

Effect of Surface Roughness and Residual Stress on Fatigue Performance of Ti-6Al-4V

Ruminda J. Wimalasiri

Abstract: Currently, manufacture of surgical implants has become the largest application of Ti-6Al-4V with aerospace, nuclear and automotive applications. One significant concern is the risk of in-vivo fatigue failure, which can lead to severe medical complications and the need for revision surgery. Due to these premature failures, implant manufacturers have been required to provide substantial financial compensation to affected patients. Examining in-vivo failures of medical implants confirm the influence of surface defects and residual stresses. The surface roughness may act as defects which influence the crack initiation, then the propagation catalyst by residual stresses. Due to manufacturing practices, the surface defects and residual stress states change over. This study focuses on the effect of the manufacturing practices on the surface roughness and the residual stresses, thereby to the life of hip prosthesis made of Ti-6Al-4V. Surface roughness and residual stress of manufacturing stages were investigated. Hourglass shaped samples were prepared adhering to the exact similar conditions to the actual implant manufacturing and rotating-bending fatigue tests were conducted. A clear variation of surface roughness and stress states were identified due to manufacturing practices and considerable variations of fatigue performance were observed. A mathematical equation is derived to assess the fatigue limit of a component with known surface roughness and residual stress. Understanding the effects of manufacturing practices on fatigue performance enables recommendations for good manufacturing practices and to eliminate in-vivo fatigue failures. Ultimately the knowledge will help to predict the life of Ti-6Al-4V products.

Keywords: Fatigue performance Ti-6Al-4V, Manufacturing Process, Residual stress, Surface roughness

1. Introduction

Manufacturing components involves different types of manufacturing operations [1]. These operations can introduce residual stresses and surface microscopic defects/roughness which may remain in the final product [2]. Clearly the residual stress states and surface texture would influence the fatigue limit. This research was conducted mainly to investigate the change of the fatigue limit along with the variation of residual stress (R_S) and surface roughness (S_R). A clear relationship of R_S and S_R on the fatigue performance is not established yet, and this study proposes a validated mathematical equation to access the fatigue limit based on R_S and S_R conditions. The production process of a hydroxyapatite ceramic (H-AC) coated hip implant made of Ti-6Al-4V was investigated. The critical processes liable to induce surface roughness and residual stress, which make an implant vulnerable to fatigue failure, were identified. Rotating-bending fatigue test samples were prepared simulating exactly similar manufacturing procedures and parameters as used in actual implant manufacture. There are two main locations [3][4] in hip implants where fatigue failure is most likely to occur. They are, the Neck region and the Cone region, as shown in Figure 1 (a) and (b), respectively. Figure 2 illustrates the main manufacturing practices involved in manufacturing the neck and cone regions of the hip implant.

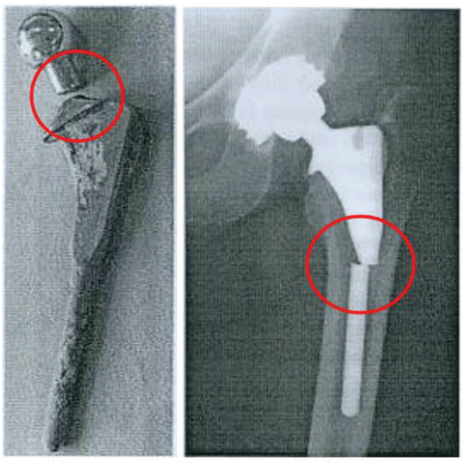

(a) (b)

Figure 1 - (a) Hip implant failed in neck region [5], (b) Hip implant failed at distal stem cone region [6]

Eng. (Dr.) Ruminda J. Wimalasiri, AMIE(SL), BTech(Hons)(Eng)(OUSL), PhD (SHU, UK), Senior Lecturer, Department of Mechanical Engineering, The Open University of Sri Lanka.
Email: rjwin@ou.ac.lk
https://orcid.org/0000-0001-8368-5639

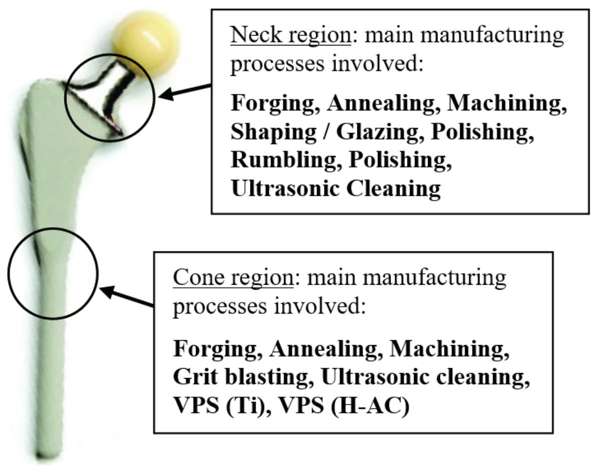

Figure 2 – Processes involved in manufacturing cone and neck regions

Following are the main manufacturing processes under consideration.

Annealing is mainly conducted to relieve stresses in the component which could be imparted by machining. Annealing was conducted at 700°C, which is the stress relieving temperature of Ti-6Al-4V alloy [7], for two hours and then air cooled.

Rumbling is a finishing operation conducted before grit blasting wherein the samples were loaded into a vibratory barrel filled with ceramic chips. When the barrel starts vibrating the surface of the samples and chips come into contact and the relative movement between chips and samples leads to scale removal.

Grit blasting is necessary prior to H-AC coating. The blasting media, chemical composition and particle size distribution and the process settings, for example, jet-pressure, jet-angle and jet-to-work distance are important parameters.

Ultrasonic cleaning: Ultrasonic cleaning is used to clean the surface of the sample, mainly to remove any embedded matter resulting from grit blasting.

Titanium and hydroxy apatite ceramic (H-AC) coating by vacuum plasma spraying (VPS): The VPS is used to coat the titanium bone coat and the H-AC upper coat to the Ti-6Al-4V parent metal in distal cone region. In VPS titanium or H-AC powder is injected into hot gas plasma that melts and projects the molten droplets at high velocity onto Ti-6Al-4V substrate to form a coating. To produce the coatings without oxidation after evacuation, the VPS spray chamber is filled with inert gas and maintained at low pressure.

2. Literature Review

In ductile polycrystalline metals, fatigue crack initiation starts from a weaker grain due to reversed shear stress associated with bands of intense slip [8]. These bands known as persistent slip bands (PSBs) were described by Thompson et. al. [9]. When loaded, localized strain density at PSB becomes higher than the adjacent matrix [10] and it has been noted that the strain within the PSB may be of the order of ten times greater than the adjacent matrix [11], which makes PSBs more susceptible for crack initiation. Fatigue life and endurance limit are illustrated by the S-N (stress-number of cycles) diagramme [12].

2.1 Total Hip Implant

The specific total hip replacement under investigation (Figure 2) is coated with H-AC. To ensure secure bonding of H-AC, the Ti-6Al-4V alloy surface is first coated with a porous titanium undercoat. Both coatings are applied by VPS to provide bond strength more than 40 *MPa*. However, the application of H-AC coating by plasma spray technique is known to have an adverse effect on the fatigue performance. Also, it is known that the thickness of the H-AC coating effects the fatigue performance of coated implants [13, 14].

2.2 Effect of Surface Roughness (S_R) on Fatigue Performance

It is known that mostly fatigue cracks initiate at the free surface, and this situation causes fatigue life sensitive to surface roughness which significantly influence S-N characteristics [15, 16]. Itoga et. al. [15] have investigated the variation of fatigue performance due to surface defects such as surface scratches, machine marks and dent-like features which roughen the surface. It has been shown that very high strength steels generally show a step wise S-N curve consisting of two parts, short life regime around 10^5 cycles and long-life regime more than 10^7 cycles (Figure 3).

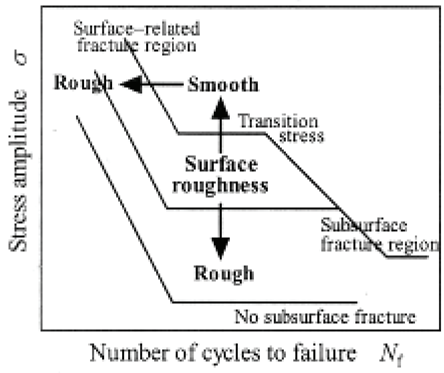

Figure 3 – Schematic diagram of the effects of surface roughness on S-N characteristics [15]

Maiya [96,18], tried to characterize surface roughness and correlate it to fatigue crack initiation using hourglass shaped fatigue samples of stainless steel. He formulated a relationship for N_o (crack initiation life), $N_o = A(surface\ roughness\ parameter)^{-\alpha}$, where A and a are constants. Figure 4 illustrates the relationship.

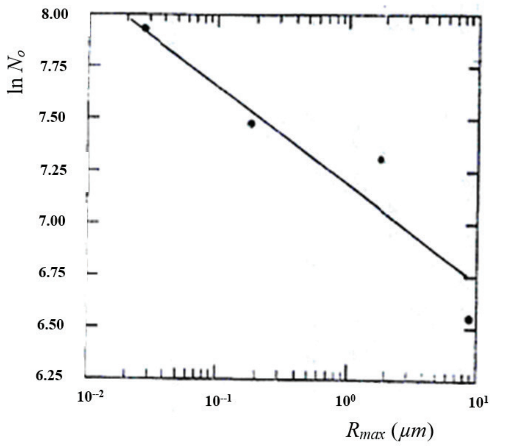

Figure 4 - Fatigue crack initiation life vs. maximum depth of surface roughness [16]

Murakami et. al. [17,18] proposed an equation for the prediction of the fatigue limit of specimens with small defects as,

$$\sigma_{w,p} = \frac{1.43(HV + 120)[(1 - R)/2]^{\alpha}}{\left(\sqrt{area}\right)^{1/6}}$$

where $\sigma_{w,p}$ is the predicted fatigue life (MPa), HV the Vickers hardness (kgf/mm^2), the square root of defect area projected onto the principal stress plane (μm), R is the stress ratio and a is given by $0.226 + HV \times 10^{-4}$.

2.3 Residual Stresses and Their Effects on Fatigue Performance

Residual stress is the internal stress existing in a body that is under no external loads. It is due to the localized plastic straining due to various loading conditions. Residual stress can have a significant influence on the fatigue life of an engineering component [19]. It is well known that near surface tensile residual stress tends to accelerate the initiation and the growth phases of the fatigue process while compressive residual stress close to a surface prolongs the fatigue life by retarding the fatigue crack growth rate [20,21,22]. Starting from the bar stock material through to the finished product, the medical implants have been subjected to various loads and stresses during manufacturing which can introduce plastic strain within the component which creates residual stresses. The residual stresses are induced by the coating deposited by the plasma spraying [23,24]. It is therefore important to investigate the introduction of residual stresses by different manufacturing processes and study the effects. Figure 5 [25] shows the interaction between peak residual stresses against fatigue strength of Ti-6Al-4V alloy under different manufacturing practices.

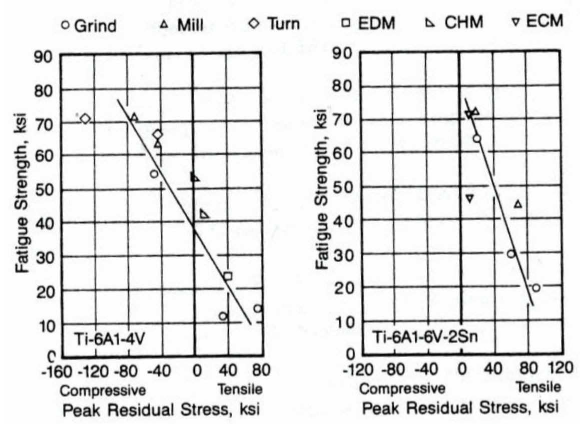

Figure 5 - Correlation between fatigue strength and peak residual stress for Ti-6Al-4V and Ti-6Al-4V-2Sn materials [25]

These undue residual stresses can be relieved, and the specifications of stress relieve heat treatments are well documented in texts and are given in Table 1 [7].

Table 1 - Stress relief heat treatment specifications for Titanium alloys

Alloy	*Stress relief*		
	Temp. (Co)	Time (h)	Cooling
Commercially pure Ti	480-600	0.25-1	air
Alpha	540-650	0.25-4	air
Near Alpha	480-700	0.25-4	air
Alpha-Beta	480-700	0.25-4	air
Beta	675-760	0.1-0.5	air

2.4 X-ray Diffraction (XRD) Technique for Residual Stress Measurements

There are different techniques used in measuring residual stress. Some are destructive techniques such as hole drilling and others are non-destructive techniques such as X-ray diffraction (XRD) and neutron diffraction [26,27], where each technique has its own advantages and disadvantages. Out of these, X-ray diffraction is the most used non-destructive technique for residual stress measurements [20,28,29].

3. Methodology

Figure 6 illustrates the main features of the study.

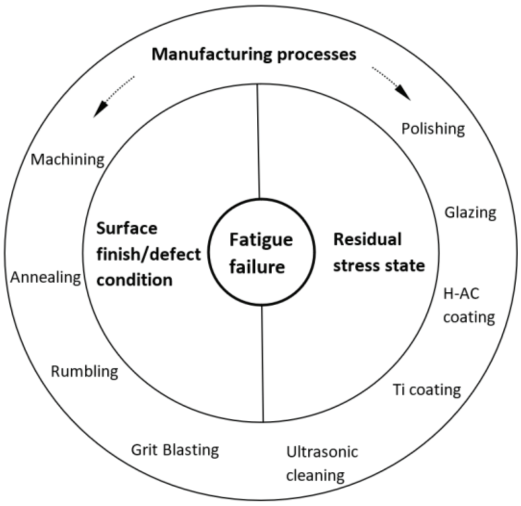

Figure 6 – Illustration of the Methodology

The rotating-bending fatigue tests were mainly conducted in two phases. Phase-1 tests were to understand the general fatigue behaviour of Ti-6Al-4V implant grade material. Samples prepared to specific surface roughness and residual stresses. Phase-2 fatigue testing was carried out to assess the influence of the manufacturing practices on fatigue performance. Then hourglass shaped fatigue test samples were prepared by the same manufacturing equipment, adhering to the exact manufacturing processes and parameters of which the actual implant manufacturing, and inspections were carried out at the quality division as per actual implants' quality checkup routines. These practices ensure the surface of the test samples is identical to the actual implant. The residual stress magnitude and the surface roughness were examined in every sample before putting to the fatigue testing. The relevant S-N curves were produced.

Phase-1 investigation consists of samples prepared in four different surface roughness states, 0.2*μm*, 6*μm*, 21*μm* and 52*μm*, each having two subsets: annealed (A) and other without-annealing (WA).
Phase-2 investigation followed the manufacturing processes involved in actual cone and neck regions of the implant. The cone region is manufactured in two ways, and it was investigated under Route-1 and Route-2, and the neck region manufacturing process is named as Route-3.
Rotating-bending samples (Figure 7) were prepared by turning 12 *mm* bar stock material to a nominal diameter of 8 *mm* using CNC turning machines. The roundness of hourglass section was inspected and ensured against a shadowgraph.

3.1 Surface Roughness Measurements

A Taylor-Hobson Talysurf-120L stylus type apparatus, with a 2 *μm* stylus tip radius, was used. Measurements were taken over a nominal 5 *mm* length using 0.8 *mm* cut off filter. Four readings were taken along the longitudinal direction around the sample at 90^{o} angular intervals as shown in Figure 7 and these positions are numbered as 1, 2, 3 (on the other side of the Figure) and 4.

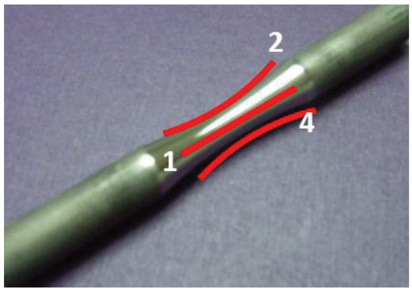

Figure 7 – Locations at which surface roughness measurements were taken from fatigue samples

A typical surface profile of a machined sample obtained from the Talysurf is shown in Figure 8.

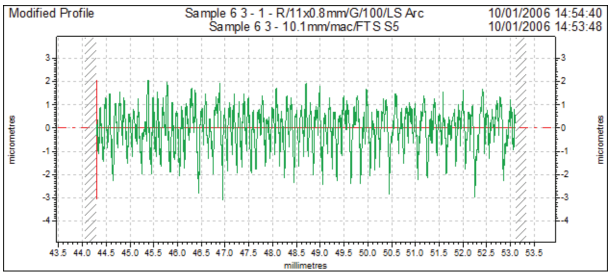

Figure 8 – Typical surface profile of a machined sample obtained from Talysurf

The surface roughness was noted as three measuring parameters, namely Ra - average roughness, Rp(max) - maximum peak height and Rv(max)- maximum valley depth.

3.2 Residual Stress Measurements

By XRD technique the residual stress status on critical area (Figure 9) of rotating-bending fatigue test samples was measured. Samples were cleaned thoroughly with IMS or acetone before measurements.

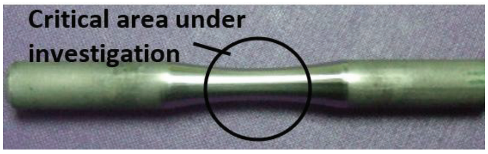

Figure 9 – Critical area of the specimen where stress measurements were conducted

XRD Apparatus: The Philips PW3040 X'Pert Pro XRD apparatus, shown in Figure 10, was used. The apparatus is subjected to periodic calibration. Copper X-ray tube was used, since copper tube gives more depth of penetration for titanium compared to Cr, Fe and Co tubes, which is about 6μm. Philips X-celerator type detector was used, which is most suitable for shorter wave lengths, texture measurements and rapid data collection.

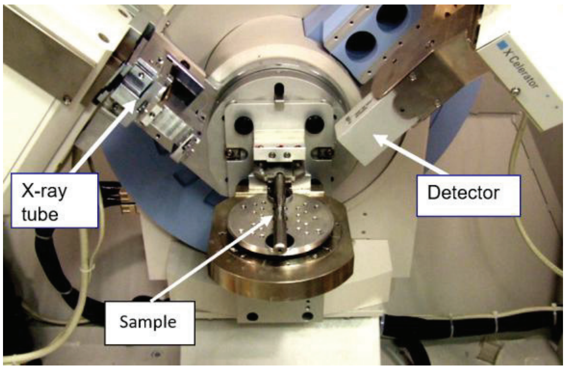

Figure 10 – X-ray diffraction apparatus with hourglass sample fixed to sample stage

Uniaxial sin2θ method was used for stress analysis. To find the most appropriate 2θ, a full scan was conducted over 180^0. The recommended 2θ angle for Ti alloys is around 139.4^0 and the lattice plane is {213}. For pure Titanium the recommended peak is at 138.46^0. But after the complete scan it was identified that for Ti-6Al-4V implant grade alloy, the corresponding peak is slightly shifted to around 142^0. Therefore, the 2θ scan was adjusted to start from 138^0 to 146^0 to cover the peak at 142^0.

To optimising scan duration, to reduce the uncertainty within residual stress measurements and to improve the goodness of fit rather than the statistical quality of the diffraction peaks, most suitable method is to increase the number of ψ measurement tilts rather than the scan time within each peak. But scan time of the peak also need to be optimized to obtain an accurate stress measurement. A total number of nine ψ angles were used. These angles were selected to cover both positive and negative quadrants. Tests were carried out to investigate the optimum time duration to obtain a more stable and accurate stress reading. The results obtained from scans conducted for 5 *hrs*, 10 *hrs*, 15 *hrs* and 20 *hrs* are given in Table 2 and Figure 11. 15hrs and 20hrs scans give almost similar values, where the graph flatted out after 15hrs. It finalizes that the most appropriate duration for stress measurement as 15 *hrs*.

Table 2 – Stress results of the investigation of scan duration

Scan duration (*hrs*)	Stress measurement (*MPa*)
5	- 442.3 ± 211
10	- 345.6 ± 79
15	- 301.8 ± 45
20	- 301.3 ± 23

After optimising the scan duration for 15hrs, repeatability of XRD measurements was investigated. The measurements were taken at the same location of the sample using identical software and hardware settings as used in all other stress measurements. The results are given in Table 2 and Figure 11. The repeatability of residual stress measurements is very good since the error is less than 1% (Table 3).

Table 3 – Results of repeatability testing scans.

Scan duration (*hrs*)	Stress measurement (*MPa*)
15	- 301.8 ± 45
15	- 302.1 ± 50

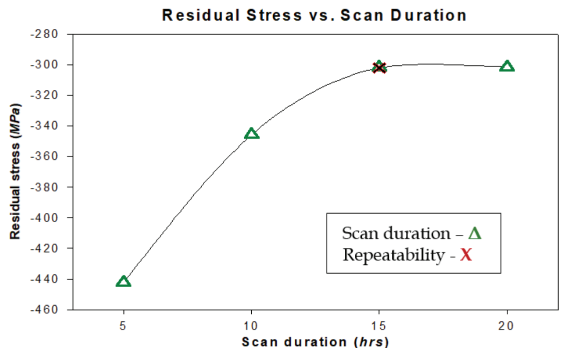

Figure 11 - Stress results conducted to optimize the and measurement repeatability

4. Results

The variation of the F_L in Phase-1, for S_R values of 0.2 *μm*, 6 *μm*, 21 *μm*, 52 *μm*, are illustrated in Figures 12, 13, 14, 15, respectively, with respective R_S values. For Phase-2, Routes 1, 2 and 3 are shown in Figure 16, Figure 17 and Figure 18, respectively. Vertical arrows represent the variation of fatigue limits, and the difference of fatigue limit (in *MPa*) is indicated in square brackets. Fatigue limit (in *MPa*) at each stage is noted in the box.

Coating process (Ti and H-AC) was omitted since the surface roughness and the residual stress value do not represent the actual values of the parent material. The results indicated in Table 4 have been used for investigation.

In Figure 16, the fatigue limit of annealed (Stage-A) sample is 365 MPa. Rumbling (Stage-B) increases the fatigue limit by 220MPa to 585MPa. Grit blasting (Stage-C) decreases fatigue limit to 523 MPa, which is a reduction of 62MPa. The fatigue limit remains unchanged after ultrasonic cleaning (Stage-D). Titanium coating (Stage-E) has only a minor effect on fatigue performance where it reduces the fatigue limit by only 6 MPa. However, H-AC coating process (Stage-F) decreases the fatigue limit by a considerable margin, notably 107 MPa. After H-AC coating the fatigue limit is 410 MPa and this is further reduced to 218 MPa after final annealing (Stage-G).

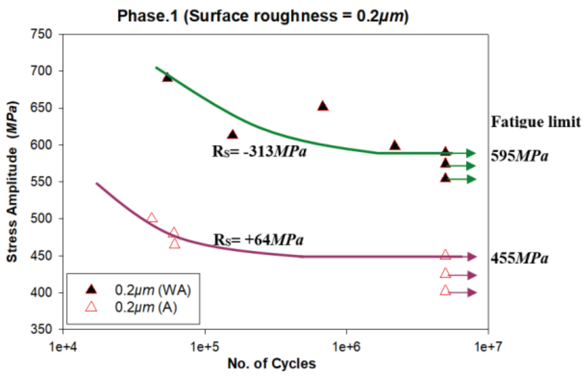

Figure 12 - Fatigue curves of samples finished to a surface roughness of 0.2μm

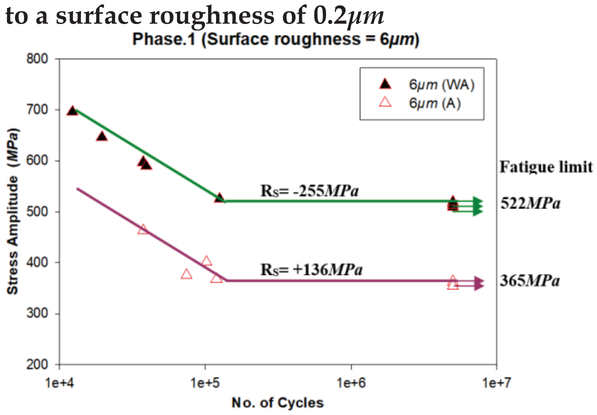

Figure 13 - Fatigue curves of samples finished to a surface roughness of 6μm

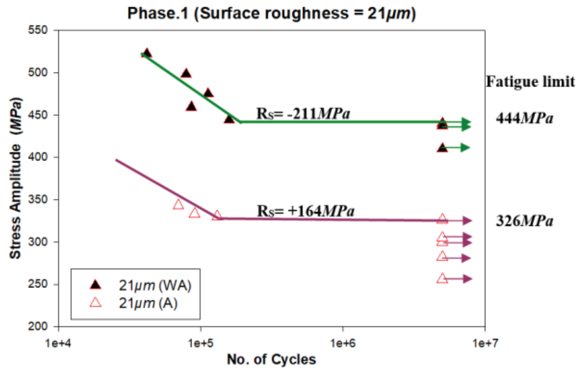

Figure 14 - Fatigue curves of samples finished to a surface roughness of 21μm

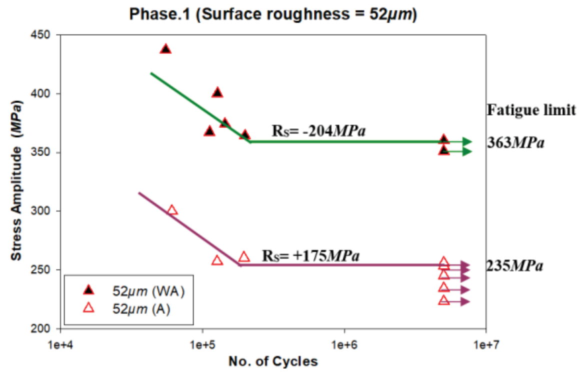

Figure 15 - Fatigue curves of samples finished to a surface roughness of 52μm

Table 4 - Variation of F_L against S_R and R_S

No.	Surface Roughness S_R - (μm)	Residual Stress R_S - (*MPa*)	Fatigue Limit F_L - (*MPa*)
	Phase-1		
1	0.2 (WA)	-313	595
2	0.2 (A)	64	455
3	6 (WA)	-255	522
4	6 (A)	136	365
5	21 (WA)	-211	444
6	21 (A)	164	326
7	52 (WA)	-204	363
8	52 (A)	175	235
	Phase-2	Route-1	
9	6.6	136	365
10	40	-431	585
11	47	-308	523
12	46	-309	523
	Phase-2	Route-2	
13	6.2	-424	682
14	51	-311	510
15	50	-315	510
	Phase-2	Route-3	
16	4.2	-436	712
17	13.1	35	345
18	5	-392	613
19	0.68	-337	643
20	0.68	102	599

Variations of the Fatigue limit with the S_R and R_S variations could be clearly examined from these S-N diagrammes.

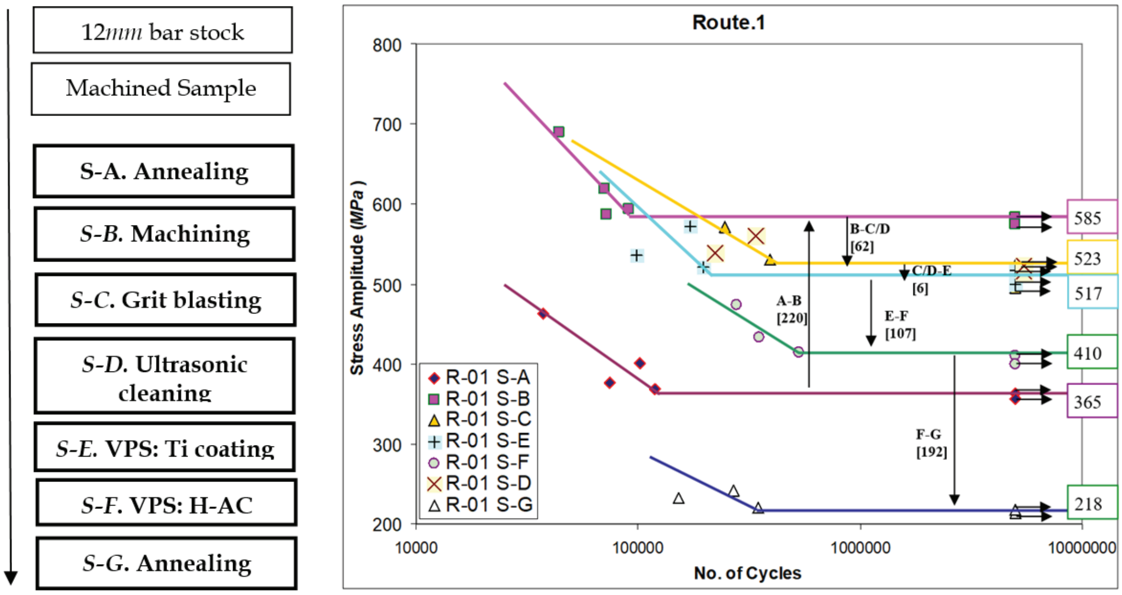

Figure 16 – Fatigue endurance limits at each stage for Route 1

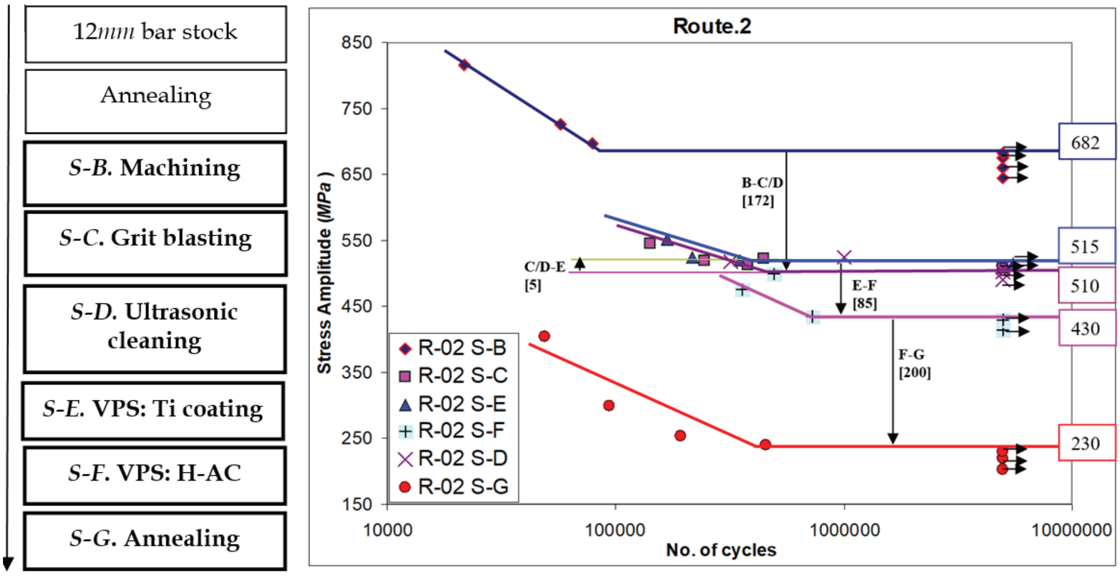

Figure 17 – Fatigue endurance limits at each stage for Route 2

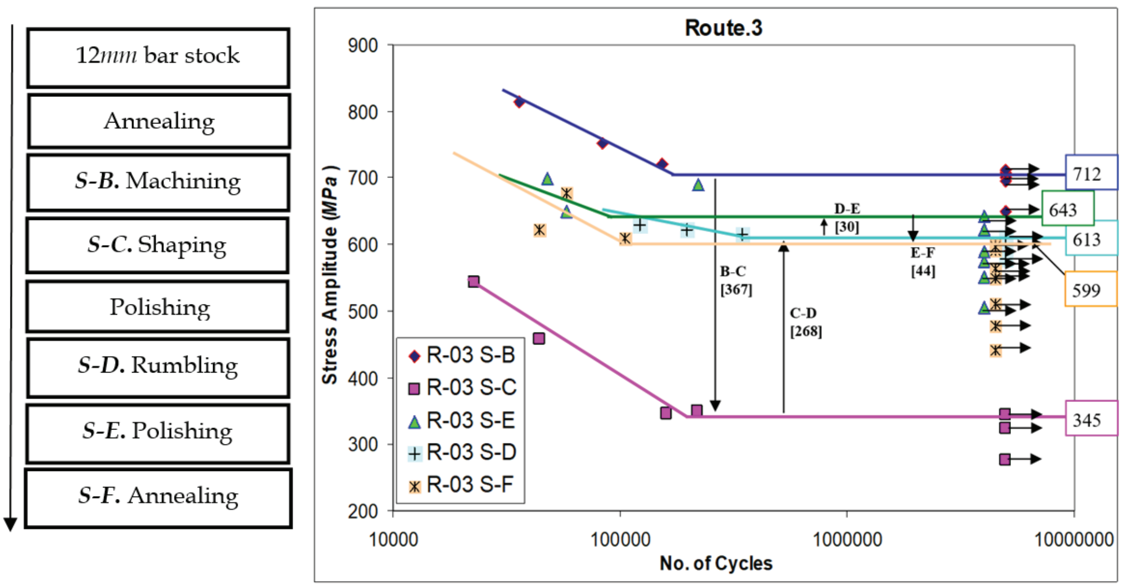

Figure 18 – Fatigue endurance limits at each stage for Route 3

5. Discussion

The variation of F_L against R_S and S_R is given Table 4 and illustrated in Figures 19 and 20 for Phases 1 and 2, respectively. Observing the distributions of data, F_L is decreasing with the increase of S_R and R_S. It is difficult to visualise a relationship of variation of F_L with both residual stress and surface roughness. However, an attempt has been made to formulate a relationship between these three parameters. The range of data covering each variable is,

Surface roughness (S_R) : 0.2 *μm* to 52 *μm*
Residual stress (R_S) : +175 *MPa* to -436 *MPa*
Fatigue Limit (F_L) : 225 *MPa* to 704 *MPa*

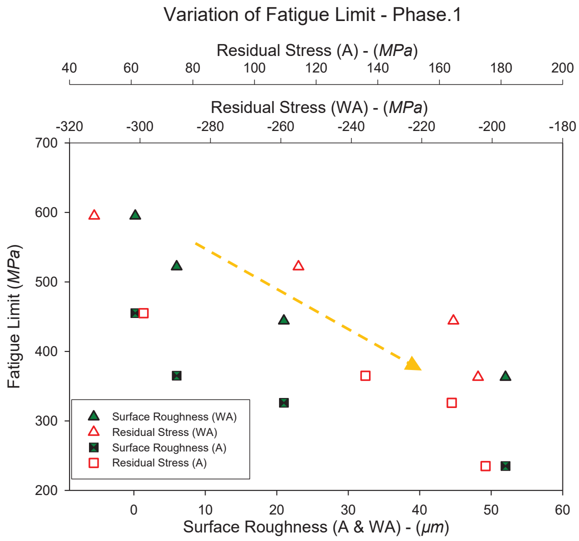

Figure 19 – Variation of fatigue limit with surface roughness and residual stress levels of the sample under Phase-1

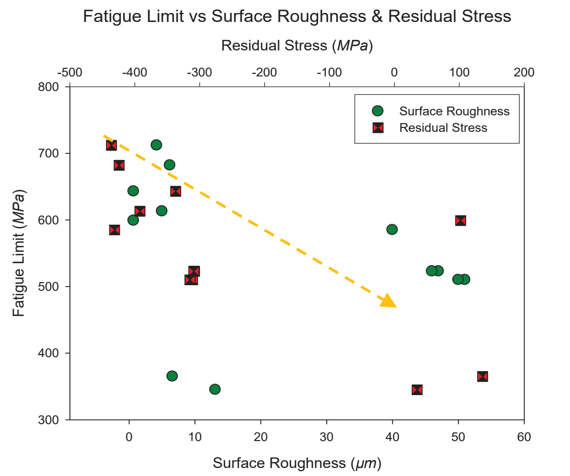

Figure 20 – Variation of fatigue limit with surface roughness and residual stress levels of the sample under Phase-2

The F_L of the samples at each stage varies with S_R and R_S values.

i.e. $F_L = f\,(S_R, R_S)$

By considering R_S and S_R as independent variables and F_L as the dependent variable, it is assumed that the relationship between F_L, S_R and R_S is in the form of,

$$F_{L\,i} = x + y \cdot R_{S\,i} + z \cdot S_{R\,i} \quad (i = 1, 2, \ldots..) \qquad \ldots(1)$$

where x, y and z are constants. Multiple regression analysis, which is a statistical analysis technique used to examine the relationship between one dependent (response) variable and two or more independent (predictor) variables, is used to derive the relationship and to test the dependency of F_L on R_S and S_R. To test the dependency, two null hypotheses (NH) and two alternative hypotheses (AH) are considered, which are,

NH 1 - $y = 0$; i.e. F_L does not depend on S_R
AH 1 - $y \neq 0$; i.e. F_L does depend on S_R

NH 2 - $z = 0$; i.e. F_L does not depend on R_S
NH 2 - $z \neq 0$; i.e. F_L does depend on R_S

The multiple regression output obtained using 'Minitab' software for the data in Table 4 is as follows:

```
The regression equation is;
FL = 474 - 0.485 RS - 2.85 SR

Predictor        Coef    SE Coef       T     P (Pivot)

Constant       473.67      20.77   22.80     0.000
RS           -0.48474    0.06001   -8.08     0.000
SR            -2.8517     0.6444   -4.43     0.000

S = 58.8232   R-Sq = 81.8%   R-Sq(adj) = 79.7%


Analysis of Variance

Source           DF        SS        MS        F        P
                                                   (Overall Pivot)
Regression        2    264801    132400    38.26      0.000
Residual Error   17     58823      3460
Total            19    323624

Unusual Observations
Obs   RS     FL     Fit   SE Fit   Residual   St Resid
 12  102  599.0   422.3     23.7      176.7      3.28R
```

The significance of the relationship between F_L, S_R and R_S are assessed by the P (pivot) value. Smaller the pivot value (zero or close to zero), higher the significance of the relationship (i.e. if the corresponding pivot value for R_S is zero, it indicates the existence of a significant relationship between R_S and F_L). The overall P value of the regression output is zero, concluding the overall model is highly significant. The residual stress value is highly significant in determining the fatigue limit. The pivot of S_R is also zero. So, null hypothesis 2 can be rejected and alternative hypothesis 2 is accepted, i.e. the surface roughness is also highly significant in determining the fatigue limit.

The derived relationship between F_L, S_R and R_S is,

$$F_L = 474 - 0.485\, R_S - 2.85\, S_R \qquad \ldots(2)$$

The fatigue limit values determined from equation (2) are compared with experimental data shown in Figure 21.

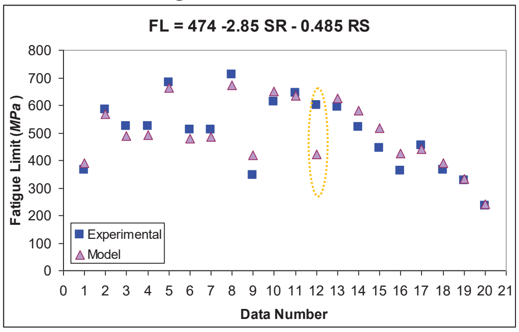

Figure 21 - Comparison of the fatigue limit values calculated from derived equation (2) with the experimental results

It can be seen that a good correlation is observed except for data point no. 12. Data point no.12 represents Stage-F in Route-3 (final annealing stage). This stage does not take place in the actual implant manufacturing process. Hence it is an outlier. With the exception of data point no.12, the average difference between the experimental and model values shows a variation of around 8.3%.
Further multiple regression results show that a more accurate model can be obtained by eliminating data point no.12. The relationship derived is,

$$F_L = 445 - 2.41\, S_R - 0.538\, R_S \qquad \ldots(3)$$

The multiple regression output for equation (3) is also checked by Minitab and the regression result concludes a highly significant relationship between F_L with S_R and R_S and is more accurate than equation (2). The distribution of experimental and calculated values from equation (3) for fatigue limit are shown in Figure 22 and Figure 23.

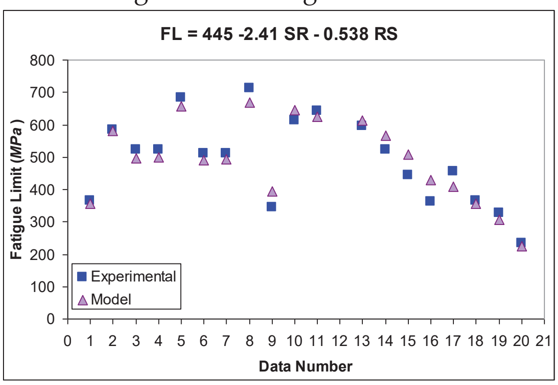

Figure 22 - Comparison of the fatigue limit values calculated from equation (3) with the experimental results

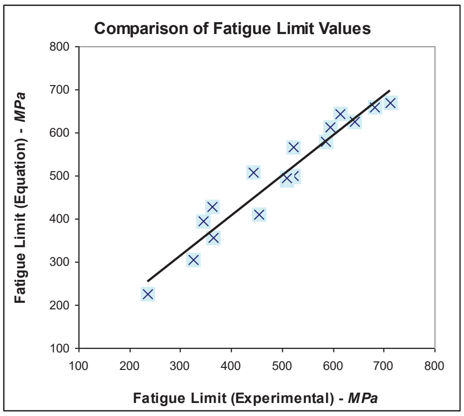

Figure 23 - Comparison of the fatigue limit values calculated from equation (3) with the experimental results

The calculated and experimental values for the fatigue limit differ in accuracy by around 5.9%. The accuracy of Phase-2 (actual implant manufacturing processes) test results is better, being 4.6%. Figure 22 and Figure 23 show an existence of a very good agreement between the experiments and the model predictions. Equation (3) is recommended for determining the fatigue limit of components with known residual stress and surface roughness values.

6. Conclusions

1. Ti coating process has almost no effect on fatigue performance.
2. H-AC coating process has strong negative influence on fatigue performance.
3. The machining stages in Route-2 / Stage-B (6.2 μm) and Route-3 / Stage-B (4.2 μm) show a difference in fatigue limit. The only difference in the processes is the depth of final cut which is 0.2 *mm* in Route-2 and 0.1*mm* in Route-1, hence reflects the importance of adhering to appropriate cutting parameters and also the effect of the process to R_S and thereby to the fatigue performance.
4. These machined samples (Stage-B, both in Route-1 and Route-2) indicate unexpected higher fatigue limits compared to other samples. Since the surface finish is less than the average grain size (7 μm) the initiation defect is within the first grain and will have to overcome the initial microstructural barrier, which can be one reason for the higher fatigue limit. Further investigations are required to fully quantify this behaviour.
5. The proposed empirical equation (3) can be accurately used to assess the F_L of the implant grade Ti-6AL-4V material for

different surface roughness and residual stress conditions.

Acknowledgement

Author wishes to acknowledge the immense guidance given by Dr. Upul S. Fernando, Prof. Robert Akid and Dr. Anita Clark.

References

1. Singh, S., Trikha, S, P., Edge, A. J., Hydroxyapatite ceramic-coated femoral stems in young patients - A prospective ten-year study, *J Bone Joint Surg*, 2004; 86-B, pp. 1118-23.
2. Kalpana, S. K., Biomaterials in total joint replacement. Colloids and Surfaces B: *Biomaterials* 39, 2004; pp. 133-142.
3. Charnley, J., Factors in the Design of an Artificial Hip Joint, *Proc Instn Mech Engrs*, 1966-67, Vol. 181 Pt 37, P2.
4. Sitting, C., Textor, N., Spencer, N. D., Surface characterization of implant materials c.p. Ti, Ti-6Al-7Nb and Ti-6Al-4V with different pertreatments, *Journal of Materials in Medicine*, 1999; 10, pp. 35-46.
5. Organ-Hough, C. V. J., Tavakkolizadeh, A., Case Report, Fatigue Failure of the Femoral Component of a Cementless Total Hip Arthroplastry, *The Journal of Arthroplasty*, 2004; Vol. 19, No. 5, pp. 658-60.
6. Sharma, D. K., Stuart, B., Stuart, C., Brian, L., Fracture of fully hydroxyapatite-coated titanium femoral stem of a total hip replacement-a report of 3 cases, *Acta Orthop Scand*, 2004; 75 (6), pp. 768-71.
7. Bolton, W., Newnes Engineering Materials Pocket Book, Third Edition, Newnes, ISBN 0-7506-4974-7.
8. Fatigue and Fracture, ASM handbook, Volume 19, ASM International, 1996; ISBN 0-87170-385-8.
9. Brown, L. M., Ogin, S. L., Role of Internal Stress in the Nucleation of Fatigue Cracks, Theory of Materials Group, University of Sheffield.
10. Irwin, G. R., Analysis of stresses and strains near the end of a crack traversing a plate, *Journal of Applied Mechanics*, 24, pp. 361-364.
11. Zang, W., Short Fatigue Crack Behaviour Under Different Loading Conditions, Ph.D thesis, 1991, University of Sheffield.
12. Wohler, A., (1860) Versuche uber die festigkeit dev eisenbahnwagenachsen, Seitschrift fur Bauwesen 10; English Summary (1867), Engineering, 4, pp. 160-1.
13. Lynn, A. K., DuQuesnay, D. L., Hydroxyapatite coated Ti-6Al-4V, part 1: The effect of coating thickness on mechanical fatigue behaviour, *Biomaterials*, 23, 2002; pp. 1937-46.
14. Evans, S. L., Gregson, P. J., The effect of plasma-sprayed hydroxyapatite coating on the fatigue properties of Ti-6Al-4V, *materials letters*, 1993; 16, pp. 270-4.
15. Itoga, H., Tokaji, K., Nakajima, M., Ko, H. N., Effects of surface roughness on step-wise S-N characteristics in high strength steel, *International Journal of Fatigue*, 2003; 25, pp. 379-85.
16. Maiya, P. S., Geometrical characterization of surface roughness and its application to fatigue crack initiation, *Material Science and Engineering*, 1975, 21, pp. 57-62.
17. Murakami, Y., Endo, M., Effects of defects, inclusions and in homogeneities on fatigue strength, *Int J Fatigue*, 1994; 16, pp. 163-82.
18. Murakami, Y., Takahashi, K., Yamashita, A., Quantitative evaluation of the effect of surface roughness on fatigue strength (effect of depth and pitch of roughness), *Trans Jpn Soc Mech Rng*, 1997; A63, pp. 1612-9.
19. Suresh, S., Fatigue of Materials, 2nd Edition, University of Cambridge, Cambridge, 1998; ISBN 0-521-57847-7.
20. Handbook of Residual Stress and Deformation of Steel, ASM International, ISBN 0-87170-729-2.
21. Webster, G. A., Ezeilo, A. N., Residual stress distributions and their influence on fatigue lifetimes, *Int J Fatigue*, 2001; Vol. 23, Sup. 1, pp. 375-83.
22. Yang, Y. C., Edward, C., Influence of residual stress on bonding strength and fracture of plasma-sprayed hydroxyapatite coatings on Ti–6Al–4V, *Biomaterials*, July 2001; Vol. 22, Issue 13, pp. 1827-36.
23. Elsing, R., Knotek, O., Balting, U., The influence of physical properties and spraying parameters on the creation of the residual thermal stresses during the spraying process, *Surface and Coatings Technology*, 1990; 41, pp. 147-56.
24. Paul, S. P., X-ray Diffraction Residual Stress Techniques, Metals Handbook, 10, Metals Park, OH, American Society for Metals, 1986, pp. 380-392.
25. Fatigue Design Handbook, Second Edition, Society of Automotive Engineers, Inc., 1988; ISBN 0-89883-011-7.
26. Withers, P. J., Bhadeshia, H. K. D. H., Residual stresses, Part 1 - Measurement techniques. *Material Science and Technology*, April 2001; Vol.17, pp. 355-65.
27. Paul, S. P., Current Applications of X-ray Diffraction Residual Stress Measurement, ASM International, Materials Park, OH, 1996, pp. 103-110.
28. Middleton, J. C., Residual Stress and X-rays, *NDT International* [0308-9126], 1987; Vol.20, Iss. 5, pp. 291-4.
29. Cullity, B. D., Stock, S. R., Elements of X-ray diffraction, Upper Saddle River, NJ: Prentice Hall, 2001; ISBN 0-20161-091-4.